

**Annual Cycle of Southeast Asia - Maritime Continent Rainfall and
the Asymmetric Monsoon Transition**

C.-P. Chang and Zhuo Wang

Department of Meteorology, Naval Postgraduate School, Monterey, California

John McBride

Bureau of Meteorology Research Centre, Melbourne, Australia

Ching-Hwang Liu

Department of Atmospheric Sciences, Chinese Culture University, Taipei, Taiwan

June 2, 2004

Corresponding author: Dr. C.-P. Chang, Department of Meteorology, Naval Postgraduate School, Code MR/Cp, Monterey, California 93943.
E-mail: cpchang@nps.edu

Abstract

In general the Bay of Bengal, Indochina Peninsula and Philippines are in the Asian summer monsoon regime while the Maritime Continent experiences a wet monsoon during boreal winter and a dry season during boreal summer. However, the complex distribution of land, sea and terrain results in significant local variations of the annual cycle. This work uses historical station rainfall data to classify the annual cycles of rainfall over land areas, the TRMM rainfall measurements to identify the monsoon regimes of the four seasons in the entire Southeast Asia, and the QuikSCAT winds to study the causes of the variations.

The annual cycle is dominated largely by interactions between the complex terrain and a simple annual reversal of the surface monsoonal winds throughout all monsoon regions from the Indian Ocean to the South China Sea and the equatorial western Pacific. The semiannual cycle is comparable in magnitude to the annual cycle over parts of the equatorial landmasses, but only a very small region reflects the twice-yearly crossing of the sun. Most of the semiannual cycle appears to be due to the influence of both the summer and the winter monsoon in the western part of the Maritime Continent where the annual cycle maximum occurs in fall. Analysis of the TRMM data reveals a structure whereby the boreal summer and winter monsoon rainfall regimes intertwine across the equator and both are strongly affected by the wind-terrain interaction. In particular the boreal winter regime extends far northward along the eastern flanks of the major island groups and landmasses.

A hypothesis is presented to explain the asymmetric seasonal march in which the maximum convection follows a gradual southeastward progression path from the Asian

summer monsoon to the Asian winter monsoon but a sudden transition in the reverse. The hypothesis is based on the redistribution of mass between land and ocean areas during spring and fall that results from different land-ocean thermal memories. This mass redistribution between the two transition seasons produces sea-level patterns leading to asymmetric wind-terrain interactions throughout the region, and a low-level divergence asymmetry in the region that promote the southward march of maximum convection during boreal fall but opposes the northward march during boreal spring.

1. Introduction

The region of Southeast Asian landmasses, which includes Indochina, the Malay Peninsula, and the Maritime Continent, is situated between the Asian (Indian) summer monsoon and the Asian winter (Australian summer) monsoon in both space and time. This area forms the “land bridge” along which maximum convection marches gradually from the Asian summer monsoon to the Asian winter monsoon during boreal fall (e.g., Lau and Chan, 1983; Meehl 1987; Yasunari 1991; Matsumoto 1992; Matsumoto and Murakami 2002; Hung et al. 2004). The seasonal march is not symmetric. During boreal spring the convection tends to stay near the equator as if it were blocked from moving northward. It stays until the reversed meridional thermal gradient is established when it jumps over the northern equatorial belt to mark the onset of the Asian summer monsoon.

Indochina is often considered as part of the Asian summer monsoon region while rainfall over most locations in the Maritime Continent tends to reach maximum during the boreal winter. This wet season is often related to the Australian summer monsoon (e.g., McBride, 1987) due to the proximity of the two regions. However, significant geographical variations of the seasonal march have been recognized since Braak (1921-1929, see Ramage, 1971). A main reason for these variations is the complex terrain due to islands of different sizes interspersed among the surrounding seas. The variations motivated Wyrski (1956) to divide the sea region into 12 climate subregions that were presented in Ramage (1971, Fig. 5.9). Other studies on the Indonesian rainfall climatology include Schmidt and Ferguson (1951), Sukanto (1969) and McBride (1998). More recently, Hamanda et al. (2002) documented the seasonal variations of rainfall at 46 Indonesian stations during a 30-year period (1961-1990) and classified the stations

objectively into five climatological types depending on the phase and relative amplitudes of the annual and semiannual cycles of rainfall. Another approach was used by Aldrian and Susanto (2003) and Aldrian et al. (2003), who used spatial correlation among station rainfalls to divide the Maritime Continent into three subregions. All these studies showed complex geographical variations of the annual cycle of rainfall in the region.

The large variation in local rainfall over small distances indicates that high-resolution wind data are required to analyze the wind-terrain interaction of the Maritime Continent. The lack of historical high-resolution and consistent wind observations made such an analysis difficult. Furthermore, since the rainfall data used in the previous studies are all from land station reports and often concentrate only in Indonesia, a gap exists in our knowledge of the distribution of the annual cycle of rainfall in the inner and surrounding seas of the Maritime Continent as well as regions north of Indonesia.

Recently available satellite-based observations make it possible to alleviate both problems. In this study, we analyze the annual cycle of rainfall by using two types of satellite data together with historical station rainfall data sets. The Tropical Rainfall Measuring Mission (TRMM) precipitation radar data, available since late 1997, are used to enhance the analysis of the geographical variations of the annual cycle of rainfall in a domain encompassing most of Southeast Asia and the Maritime Continent. The QuikSCAT scatterometer winds, available since July 1999 at the sea surface, are used to help examination of the relationship between the monsoon-terrain interaction and the geographic variations. The result of the analysis will be used to address the cause of the asymmetric seasonal march of maximum convection during the transitional seasons.

2. Data

Two data sets of monthly station rainfall are used in this study. The first is an extension of the Indonesian rainfall data set prepared by Kirono et al. (1999) and used in Haylock and McBride (2001). This data set, hereinafter referred to as the INDO data set, contains rainfall during 1950-1997 at 63 Indonesian stations. The second is the Association of Southeast Asian Nations (ASEAN) Climatic Atlas Project (ACAP) data, furnished by the Malaysian Meteorological Service. This data set covers 935 rainfall stations in all the member nations of ASEAN during the data collection phase. The beginning dates of the stations vary, with the earliest date in each country as follows: Singapore 1875, Malaysia 1876, Indonesia 1879, Philippines 1902 and Thailand 1911. The majority of the stations start from 1951 or earlier, and almost all start from 1958 or earlier. All stations end in 1975. The two sets have overlapping observations over Indonesia between 1950-1975.

The TRMM microwave precipitation data (Simpson et al., 1996) became available November 1997. In this study, we use the data of January 1998 – December 2002 (Data for 7 – 24 August 2001 are missing). The original data at resolution of 4 km x 4 km are smoothed into a grid of 0.5° x 0.5° using the two-step filter of Leise (1982).

The QuikSCAT scatterometer winds (Liu, 2002) cover the period January 1999 – December 2002. These are scatterometer winds at the sea surface at 25 km × 25 km resolution. On a typical day the available data covers 75% of the equator and increased percentage of area away from the equator. These data are used to produce monthly mean winds at the sea surface.

3. Analysis based on station rainfall reports

a. Monthly mean rainfalls

As background, the large influence of the annual cycle can be seen clearly in Fig. 1, which includes monthly mean rainfall from both the INDO and ACAP data for January, April, July, and October (Chang et al. 2004b). For this figure all station rainfall data have been interpolated to a $0.5^\circ \times 0.5^\circ$ grid using the methodology of Cressman (1959). This figure should be interpreted with reference to the data locations or stations in Fig. 2. The stations north of 10°N experience a wet season during July and October and those south of 5°S have their wet season during January and April. Rainfall amounts are high throughout the region with individual monthly totals on the order of 300 to 500 mm. Most of the region experiences a distinct dry season at some time of year, with the exception being parts of Borneo and New Guinea, which have high rainfall year round. (Place names are shown in Fig. 2). The seasonal shift is such that in January the center of mass of the heavy rainfall is south of the equator while in July the rainfall is northward of 10°N . This is associated with the seasonal migration of the Inter-Tropical Convergence Zone (ITCZ) in the region, as has been documented by Johnson and Houze (1987), Waliser and Gautier (1993), McBride et al (1995) and Qian and Lee (2000).

The other major feature in Fig. 1 is the existence of strong rainfall gradients existing at all times of the year; for example, notice the east-west gradients of rainfall across the Philippines in January and across the Malay Peninsula in April. As will be discussed below, these patterns result largely from the interaction between the high topography in the region and the moisture-bearing low level monsoon flow, whereby rainfall is enhanced when the flow is lifted on the upstream side of a mountainous island or

Peninsula. Conversely the flow on the downstream side experiences a rainfall minimum associated with a lee or rain-shadow effect.

b. Annual cycles

The annual cycle and semiannual cycle modes are the first two harmonics of the climatologically averaged annual rainfall variation at each location. Because only monthly mean station rainfall data are available, each time series has only 12 data points. Figure 2 shows the annual cycle mode at land stations, with the amplitude represented by the length of each arrow and the phase shown as a 12-month clock with a northward arrow indicating maximum rainfall in January. The arrow rotates clockwise with eastward, southward and westward arrows indicating April, July and October, respectively. This figure is examined along with the mean QuikSCAT winds in January and July shown in Fig. 3, which also includes the distribution of topography.

North of the Maritime Continent, data are available in two Southeast Asian regions, Indochina (Thailand stations) and Philippines (Fig. 2). In Indochina, the effect of the Asian summer monsoon is clearly indicated with most Thailand stations showing maximum rainfall around June. Over the Philippines, the Asian summer monsoon rainfall is defined at most stations in the south and west where the rainfall maximum occurs around July. These are stations on the windward side during the southwest monsoon (Fig. 3). On the other hand, most northern and eastern stations show maximum rainfall in late summer or early fall. There are two factors influencing this. A major factor for this variation is that during the peak of the southwest monsoon in July these stations are on the leeward side of the high topography on the islands. Because of the sheltering effect of the topography, they do not experience a wet monsoon at this time of year. However,

during September through December when the southwest monsoon begins its retreat, northeasterly flow occurs and these same stations are now on the windward side. At that time of year (fall-summer) there is still upward motion associated with the retreating ITCZ; so there is a late wet season associated with terrain-lifted rainfall. The second factor is that the number of typhoons peaks in September; and tropical cyclone are considered to be major contributors to rainfall in the northeastern Philippines (Coronas, 1912; Masó, 1914; Flores and Balagot, 1969). The relative contributions of these two factors are not known without further study.

The southern Philippine island of Mindanao is considered part of the Maritime Continent, based on Ramage's (1968) definition. Here, the seasonal cycle over most of the region is characterized by the summer monsoon rainfall. The exception is in its northeastern corner, where maximum rainfall occurs around November and December again as a result of the prevailing northeasterly onshore winds (Fig. 3) during the northern winter monsoon.

In Fig. 2 the distribution of the annual cycle over the Philippines appears as a counterclockwise pattern in the phase diagram, associated with a progression from a November-December maximum on the southeastern side, an August-September maximum on the northeast, and a July maximum along the western coastline. In contrast, over the western Maritime Continent from Indochina to the Malay Peninsula, phase of the annual cycle moves in a clockwise manner reflecting the seasonal march of the deep convection that follows the sun (Lau and Chan, 1983). Thus, the annual cycle maximum occurs mostly during northern fall in the Malay Peninsula and northern Sumatra and changes to around December in southern Sumatra. Over the rest of Indonesia the boreal

winter maximum in the annual cycle occurs in most places, especially in southern Borneo, Java and other islands near 10°S.

As pointed out by previous investigators (e.g., Ramage, 1971; Hamada et al., 2002), the majority of the locations south of the equator have monsoonal rainfall with a wet boreal winter and a dry boreal summer, although there are distinct exceptions. The most noteworthy exception is over the central Celebes and the Molucca area, where the maximum in the annual cycle of rainfall may occur during boreal spring and early boreal summer (Fig. 2). This has been noted by many previous investigators (e.g., Wyrski 1956; Ramage 1971; Hamada et al. 2002; Aldrian and Susanto 2003; Aldrian et al. 2003).

This “out of phase” effect is restricted to the southern coastline of the Molucca region whereas the northern coastline has its annual cycle maximum in January-February, which is closer to the phase of the larger scale region (Fig. 2). The topography of the islands is such that a mountainous ridge lies along the islands in an east-west direction. The east and south sides of the islands in the Molucca area are sheltered from the northeast monsoon winds during boreal winter, but they face the southeasterly monsoon winds that produce convergence against the terrain during boreal summer (Fig. 3). Thus, the cause of this out-of-phase behavior with the majority of the Maritime Continent appears to be the result of sheltering by the mountains during the boreal winter and orographic uplift during the boreal summer. The large variation in phasing of the annual cycle across the islands presents an excellent example of the importance of local and orographic effects at low-latitudes as was discussed by Riehl in his classical text on tropical meteorology (Riehl, 1954).

For reasons that are not entirely obvious, the upwind-lee effect seems not to apply along the Indonesian archipelago (Java and points eastward on Fig. 2). Part of the reason is that at this more southern location the boreal winter monsoon flow has a more dominant westerly component, so the flow is parallel to the long-island topography. This is not the entire explanation, however, as the island of Timor for example has an orientation whereby there should be a rain-shadow effect for some stations; but according to the data in Fig. 2, this is not observed.

c. Areas without strong annual cycles.

The discussion of Figs. 1 and 3 has brought out the very large role played by the annual cycle in Maritime Continent monthly rainfall. However, there are locations where the annual cycle is less dominant. These locations are identified in Fig. 4, in which the annual cycle amplitude and phase are plotted (black arrows) against the maximum monthly rainfall (gray arrows) for the objectively analyzed gridded-rainfall field, with the results plotted every other grid point ($1^\circ \times 1^\circ$ resolution). The maximum monthly rainfall arrows are scaled to 1:4 of the annual cycle arrows. The locations where the annual cycle is less important are delineated by a black dot, which is plotted if the amplitude of the annual cycle is no more than 40% of the maximum rainfall and if the phase difference is at least two months.

The locations where the annual cycle plays a lesser role are the eastern and central Philippines, northeast Borneo, southern Thailand and parts of the northwest end of New Guinea. Inspection of the plots for the individual months indicates the reasons for this geographic variation. In southern Thailand the wet season extends through the boreal summer (as indicated by the June orientation of the annual cycle arrow); but this

culminates in a period of intense rainfall at the end of the wet season around September (as indicated by the orientation of the “maximum month” arrow). In contrast, in northeast Borneo the reason for the less prominent annual cycle is that the rainfall tends to be well distributed over all months of the year, so the magnitude of the annual cycle arrow is small compared to that of the maximum month.

d. Areas with significant semiannual cycles.

Following the approach of Hamanda et al. (2002), we also examined the distribution of the semiannual mode of station rainfall (Fig. 5). The semiannual mode is more likely to be meaningful if it is comparable in magnitude to that of the annual cycle. In Fig. 5, the semiannual cycle is plotted at grid points where its amplitude is at least 80% of the annual cycle amplitude. The annual cycle at all grid points is also plotted for comparison. Here for the semiannual cycle mode, a vertical (north-south) bar indicates rainfall maximum in winter and summer and a horizontal (east-west) bar indicates rainfall maximum in spring and fall. Because the semiannual cycle has two maxima, each bar is centered at the grid point and points in the two (opposite) directions. The length of the bar from the center to each of the two end points has the same scale as the length of the vectors in the annual cycle mode. Thus, the entire length of the bar representing the semiannual mode is twice the length of an annual cycle vector with the same amplitude.

In general, the semiannual cycle tends to be concentrated over three areas within the equatorial zone of 3°S - 7°N. The first is west of 110°E, which is the transitional zone between summer and winter monsoon with the annual mode peaking in boreal fall. North of the equator in western Malay Peninsula – northern Sumatra, the semiannual indicators orient mostly June/December versus the annual mode that peaks around September.

Further southeast in the narrow equatorial sea region between Sumatra and Borneo, the semiannual indicators have a February/August orientation versus the annual mode peak of November. These semiannual mode indicators are normal to the annual mode vectors and suggest *the influence of both boreal summer and boreal winter rainfall*.

The second main area is in northeastern Borneo between 114°E - 120°E. The annual modes are small and the semiannual mode indicators again have a boreal summer/winter orientation, with a gradual clockwise shift from north to south. The orientation is January-February/July-August at about 3°N-4°N, March/September near 1°N-2°N, and April/October at the equator.

The few equatorial grid points define the third main area further to the east, which is the equatorial zone between 120°E - 130°E. This region covers the vicinity of the Molucca Sea and Molucca Passage, including northern Celebes and Halmahera. Here the semiannual mode indicators are oriented horizontally (March-April/September-October), suggesting the possible *effect of the twice-a-year crossing of the sun over the equator*. The double rainfall peak associated with the twice overhead crossing of the sun is sometimes considered as the classical mode for the annual cycle of tropical rainfall. One of the most significant aspects of Fig. 5 is how rarely the double rainfall peak occurs in the Maritime Continent, as it is effectively restricted to those few equatorial grid points where the semiannual mode indicators orient horizontally.

4. Monsoon regimes and transitions

The TRMM data provide complete spatial coverage for the domain, but the available data period is only five years and the data are derived from remotely sensed variables. This very small sample size makes it difficult for any composite values to attain a high

level of significance. The confidence of the composite results will have to depend on whether the results can be consistently explained by physical reasoning over many different locations. To assess the quality of the data, it is desirable to compare the TRMM data with the station rainfall data. However, a direct comparison is not possible because the two data sets do not overlap. Since the purpose of this study is analysis of the mean annual cycle, our interest is whether the annual cycle derived from the TRMM data set is consistent with that of the long-term station rainfall. Therefore, the comparison is done by first calculating the annual cycle mode of the TRMM precipitation radar (PR) data and then computing the difference (Fig. 6) between it and the annual cycle mode of the analyzed rainfall data (Fig. 4) at all land grid points. In Fig. 6 the vector direction shows the phase difference in a 12-month clock. A northward pointing arrow means the two annual cycles are exactly in phase, and a westward (eastward) pointing arrow means the TRMM PR annual cycle mode leads (lags) the analyzed rainfall mode by three months. Gray arrows mean the amplitude of TRMM PR mode is larger and black arrows mean it is smaller. In general, the phase angles are quite small (within two months). The amplitude difference is sometimes large, particularly over the Indochina Peninsula north of 10°N. Since the two data periods are not overlapping, it is difficult to conclude that any difference represents errors of the TRMM mode. On the other hand, the generally small phase differences suggest that the TRMM data are useful for the study of rainfall annual cycle over the region.

a. Regimes of boreal summer and boreal winter monsoon rainfall.

Figure 7 shows the difference in TRMM PR data between December-January-February (DJF) and June-July-August (JJA). Here the yellow-red colors show areas of

more rainfall in JJA and the green-purple colors show areas of more rainfall in DJF. Thus, this chart can be viewed as the demarcation of the boreal summer and winter monsoon rainfalls. Because of the limited duration (15 months for each season) and the narrow individual TRMM data swaths, some small scale features may be artificial, but the general patterns should reflect the mean seasonal differences. Also plotted on Fig. 7 are the DJF-minus-JJA QuikSCAT winds. From the rainfall difference, the boreal summer rainfall regime dominates north of the equator, and the boreal winter rainfall regime dominates south of the equator. The two regimes become mixed near the equator, but the extent of mixing is not symmetric. The boreal winter regime extends far northward into the boreal summer regime, whereas the southward extension of the boreal summer regime south of the equator is much more limited. Over Southeast Asia, the intrusions beyond 5°N occur in the following areas: east of the Philippines, northeast and northwest of Borneo in the South China Sea, east of Vietnam, eastern coast of Malay Peninsula, and north of Sumatra. In most of these areas the high boreal winter rainfall is due to the onshore northeasterly winter monsoon winds from the northwest Pacific and the South China Sea. These northeasterly monsoon winds are stronger than the southeasterly winds because of the intense baroclinicity over the cold Asian continent in boreal winter; a similar counterpart does not exist in the Southern Hemisphere in boreal summer. There are also very few coastal areas between 5°S -10°S that face the prevailing seasonal wind as is the case in the northern tropics.

The fact that most of the monsoon rainfall is a result of wind-terrain interactions is also readily apparent in the summer monsoon regime (warm colors in Fig. 7). The heaviest rainfall occurs on the summertime windward side of the terrain, which includes

the northeastern Bay of Bengal, the eastern Gulf of Thailand, west of the north-south oriented mountain ridge along Vietnam, and the northern South China Sea (off the western coast of the northern Philippines and the southern coast of China's Guangdong Province). It is worth noting that while heavy summer rainfall is often associated with tropical cyclones such as monsoon depressions in the Bay of Bengal, the heaviest rainfall is not along the averaged track of the cyclones, which extends northwestward to the eastern coast of India (Neumann 1993), but is near the western coast of Burma where much fewer cyclones have made landfall. In fact, the relatively lower amount of monsoon rainfall over the India subcontinent compared to the Bay of Bengal may be partly due to the wind-terrain interaction in the eastern Arabian Sea where heavy rainfall accumulates off the west coast of India (not shown). Another example of the importance of the wind-terrain interaction in the summer monsoon can be seen southwest of the Bay of Bengal, where Fig. 7 shows another extension of the boreal winter monsoon regime to the northern tropics. This winter regime just east of Sri Lanka between 5°N-10°N is in the middle of the eastern Indian Ocean where the DJF rainfall does not stand out as being particularly high in the boreal winter TRMM rainfall distribution, but rather is a minimum JJA rainfall area in the eastern Indian Ocean (not shown). This minimum is apparently due to the sheltering of the southwest monsoon by the island of Sri Lanka. As a result, the DJF-JJA difference (Fig. 7) indicates this region to be a winter monsoon regime.

The intrusion of boreal winter rainfall regime into the southern South China Sea northwest of Borneo does not occur as a result of direct onshore winds, where the northeast monsoon is parallel to the coastline. This is the vicinity of the low level quasi-

stationary Borneo vortices that are associated with the heating of the island and can develop any time of the year. During boreal winter, the northeast cold surge winds increase periodically for periods of one to several weeks and enhance the low-level cyclonic shear vorticity off the northwest coast of Borneo. As a result, the Borneo vortices are particularly active during boreal winter (e.g., Johnson and Houze 1987; Chang et al. 2003; 2004a,b). Due to the increased frequency of the Borneo vortex, the deep convection and heavy rainfall frequently extend offshore several hundred kilometers into the South China Sea during boreal winter, but much less so during boreal summer.

Over the Maritime Continent region the only significant intrusion of the boreal summer rainfall regime into the southern tropics beyond 5°S is on the south side of western New Guinea between 135°E-138°E. During both winter and summer, this area faces some onshore winds (Fig. 3). The southeasterly winds during boreal summer are stronger and have a larger angle with the southern coastline; the westerly winds during boreal winter are weaker and nearly parallel to the coastline.

Within the equatorial belt of 5°S-5°N, the mixing of the boreal winter and boreal summer rain regimes is almost entirely the result of the sheltering by the mountains and the direct onshore winds onto the complex island geography. Here, the TRMM data available over both land and water show this wind-terrain interaction within the Molucca region more completely than that identified by the station rainfall data (Fig. 2).

b. Regimes of the transitional seasons and the asymmetric seasonal march.

In this section we present the monsoon regimes during the transition seasons, boreal spring (March-April-May, or MAM) and boreal fall (September-October-November, or SON). Figure 8 is a summarized view of the monsoon rainfall in these seasons. Two steps

are taken to create this chart. In the first step, at each grid point where the MAM rainfall (green) is the maximum among the four seasons, the difference between the MAM rainfall and the higher of the summer or winter rainfall is computed. The same procedure is followed at points where the SON rainfall (yellow) is the maximum of all four seasons. The resultant values are then plotted together in Fig. 8. The QuikSCAT winds for both seasons are also plotted, with the MAM wind in black and the SON wind in red.

In Fig. 8 the SON monsoon rainfall dominates areas north of the equator, particularly the western side of the domain. The MAM monsoon rainfall dominates areas south of the equator, particularly the eastern side of the domain. Within the equatorial belt of 10°S-10°N, the area west of 114°E, or about the longitude of central Borneo, is mainly in the SON regime while the area to the east is mainly in the MAM regime. Away from the equator, significant Northern Hemisphere SON monsoon rainfall can also be found in the South China Sea and east of Philippines. Similarly significant monsoon rainfall does not exist in the Southern Hemisphere MAM regime (not shown).

As has been noted by previous investigators (e.g., Lau and Chan, 1983; Meehl 1987; Yasunari 1991; Matsumoto and Murakami 2000, 2002; Hung and Yanai 2004; Hung et al. 2004), the distribution of the transition season convection indicates that the advance of the annual cycle in space is not symmetric. The Asian summer monsoon has its maximum convection located in South Asia around India and Bay of Bengal. During boreal fall, the maximum convection moves southeastward through the eastern Indian Ocean and the South China Sea in a track that roughly follows the Southeast Asia land bridge, to reach southern Indonesia and northern and eastern Australia during boreal winter. This pattern is reflected in the annual cycle diagram (Fig. 2). However, during

boreal spring the monsoon convection does not return to the Northern Hemisphere along the same path. The maximum rainfall remains mostly south of the equator. In the western sector of the domain in the eastern Indian Ocean, it occurs to the south of 10°S and northwest of Australia, which is further south than the boreal winter convection belt. In the eastern sector of the domain it moves slightly northward in the New Guinea region. So there is no northwestward progression to retrace the path of the Asian summer to Asian winter monsoon progression.

This spring-fall convection asymmetry is apparently related to the interaction between winds and the terrain of Southeast Asia. In the northern South China Sea, the mean seasonal wind in boreal fall is northeasterly and its speed is stronger than the weak easterly during boreal spring. This contrast was noticed by Matsumoto and Murakami (2000) who related the cold surges during boreal fall to the enhanced convection in the Borneo area. The seasonal winds lead to strong convection off the coast of Vietnam in boreal fall but not in spring (Fig. 8). Similarly, strong convection occurs east of the Philippines only in boreal fall due to stronger northeasterly onshore winds. The convection in these areas is much stronger than both boreal summer and winter, even though during boreal winter the northeasterly winds are stronger. This is because during winter the colder and drier air and the lower sea-surface temperature (SST) make deep convection less likely to develop north of 10°N, so that strong winter cold surges actually produce drying conditions in northern and middle South China Sea (Chang *et al.* 2004a,b).

This fall-spring difference in winds may be traced to the difference in the sea-level pressure (SLP) distribution, which tends to have opposite signs between land and ocean

areas because of differences in surface temperatures (e.g., van den Dool and Saha 1993). The long-term mean SON-minus-MAM SLP during 1968-1996 computed from the NCEP/NCAR Reanalysis is shown in Fig. 9. Compared to boreal spring, SLP in the Northern Hemisphere during boreal fall tends to be higher over the land and lower over the ocean, and the reverse is true in the Southern Hemisphere. This pattern is seen throughout most of the global domain except for of the midlatitude storm tracks over oceanic areas, whose effect in reversing the difference sign can be confirmed by a map of spring-fall 500 hPa height difference (not shown). In this map the most conspicuous difference is the lower heights during the local fall season due to the active storms near the midlatitude jet streaks.

The SLP difference shown in Fig. 9 may be caused by two effects. Over oceans, the delayed thermal response will give a relatively warm SST in fall, which contributes to lower SLP, and a relatively cool SST in spring, which contributes to higher SLP. Over land areas, the thermal memory is very short; thus an asymmetric land-sea SLP contrast will occur between fall and spring. This asymmetry is further enhanced by the timing of the equinox. Because it occurs at approximately the 22nd day of the respective three-month seasons, the land surface temperature tends to be cooler and SLP higher during fall than during spring. In Fig. 9, this land SLP response in low and middle latitudes is largest in East Asia, with the maximum SLP difference centered in the northern China – southern Mongolia Plain. Another interesting feature in Fig. 9 is that both polar regions have the same sign, because the Arctic is water and Antarctic is land¹.

¹ In the southern high latitudes, the semiannual oscillation of SLP surrounding Antarctica (e.g., van Loon 1967) may also play a role in the lower SLP in the SON minus MAM difference.

An enlargement of the Southeast Asia and Maritime Continent domain shown in the insert to Fig. 9 is displayed in Fig. 10, with schematic sea-level winds based on the SLP gradient depicted in key areas for discussion. In these areas the pressure gradient is less susceptible to the errors introduced in the conversion of pressure from land surface to the sea level. Schematic winds based on broader-scale pressure patterns instead of actual spring-fall wind differences make the discussion somewhat qualitative rather than quantitative, but the purpose here is to derive a hypothesis for the source of the asymmetric seasonal march that is not blurred by the results of the asymmetric march. The actual wind differences already include the effect of the asymmetry within the tropical belt and it would be harder to sort out the cause-effect. The large SLP difference over East Asia leads to the stronger SON northeasterly winds in the northern South China Sea and northwestern Pacific (area A in Fig. 10), which causes the deep convection east of Vietnam and Philippines in boreal fall. In the southern South China Sea, the SLP gradient favors cyclonic flow and therefore deep convection in SON (area B in Fig. 10). This wide-spread convection in the southern South China Sea during boreal fall is not very obvious in Fig. 8 because at many points convection in boreal summer is even stronger. The convection is further enhanced by the interaction of the wind with terrain on the east coast of Sumatra and west coast of Borneo.

The enhanced convection in the eastern equatorial Indian Ocean may also be explained, at least partly, by the spring-fall SLP difference. Here the Bay of Bengal and the northern Indian Ocean have higher SLPs in boreal fall than in boreal spring, which suggests that atmosphere-ocean interaction is involved to increase the SST faster during boreal spring. One possibility is that the initially anticyclonic flow with weak winds

cause less evaporation and more solar heating at the sea surface and downwelling in the upper ocean, so as spring progresses the SST becomes higher and SLP becomes lower than during fall. However, the land-sea redistribution of mass still contributes to a lower SLP over the Bay of Bengal in boreal fall compared to surrounding land areas. The resulting difference in pressure gradient during boreal fall gives rise to cyclonic flow in the Bay of Bengal and favors increased cross-equatorial flow from the southern Indian Ocean.

The convection in and around the middle and southern South China Sea in boreal fall helps to induce southwesterly winds west of Sumatra (area C in Fig. 10). These southwesterly winds are enhanced by the tendency for cross-equatorial flow and the cyclonic flow in the Bay of Bengal. Other atmospheric and oceanic factors, such as the east-west pressure gradient across equatorial Indian Ocean, may also contribute to the development of equatorial westerly winds. These winds have two effects, both of which lead to more convection. The first is the onshore flow that causes convergence along the western coasts of northern Sumatra and the Malay Peninsula. The second is the beta effect that produces convergence in the equatorial westerlies in the boundary layer. The increased convection may further enhance the westerlies off the coast of Sumatra and make a positive feedback possible.

South of the equator, the SLP difference between Australia and the South Indian Ocean favors counterclockwise flow towards the equator (area D in Fig. 10) in boreal fall. This also enhances the cross-equatorial flow that becomes a westerly wind north of the equator, and thus increases the wind-terrain interactions on the west coast of the adjacent land areas, such as western Borneo (area B). Furthermore, the convergence of

these winds from south of the equator and the northeasterly winds in the northern South China Sea and the northwestern Pacific (area A) give rise to a broad-scale belt of convergence between the equator and 20°N during boreal fall (marked by the elliptic-shaped area in Fig. 10), which also favors convection. During boreal spring, this belt becomes a zone of low-level divergence, so convection is suppressed. The results of these various effects are that maximum convection is prevented from marching continuously from the Asian winter monsoon to the Asian summer monsoon.

5. Summary and Concluding Remarks

In this study, historical station rainfall data were used to classify the geographical distribution of the annual cycle of rainfall in the Southeast Asia - Maritime Continent region into several types, which depends on the wet season, the amplitude and phase of the annual cycle, and its importance relative to the maximum rainfall and season, and the relative importance of the semiannual cycle. Over Indonesia, the results are consistent with the gross features of Hamada et al's (2002) five-type classifications using 1961-1990 data.

The annual cycle dominates rainfall over most of the region and its phase and amplitude vary significantly. The QuikSCAT sea-surface winds show that most of these variations are due to interactions between the complex terrain and a simple annual reversal of the surface monsoonal winds. The most notable example is the effect of seasonal-varying onshore winds and the activity of low-level vortices in the South China Sea along the northwest coast of Borneo. The semiannual cycle is comparable in magnitude to the annual cycle over parts of the large islands of Sumatra and Borneo and the Malay Peninsula. Only a very small part of eastern Indonesia close to the equator

exhibits a modest semiannual variation that may be attributed to the twice-yearly crossing of the sun.

Analysis of the data reveals a clear demarcation of the boreal summer and winter monsoon regimes over the entire region, showing the two regimes intertwining across the equator. There are stronger intrusions of the winter regime northward into the summer regime due to strong northeasterly monsoon winds in the South China Sea and the western Pacific east of the Philippines. These monsoon winds produce strong onshore flow and excess rainfall along the eastern flanks of the major island groups and land masses. During boreal summer, the interaction between the southwest monsoon wind and terrain also affects strongly the distribution of the summer monsoon rainfall, with maximum rainfall occurring on the windward side of terrain in the Indian Ocean, the Indochina Peninsula, and the South China Sea.

The analysis also clearly delineates the asymmetry of the season march between boreal fall and boreal spring. During boreal fall the convection maximum occurs in the eastern Indian Ocean, Malay Peninsula and Sumatra, and southern South China Sea. This general area forms the midpoint of the path of the southeastward progression of convection from the Asian summer monsoon to the Asian winter monsoon. During boreal spring the maximum convection does not retrace the process but stays near and south of the equator. This asymmetric feature is a manifestation of the asymmetric locations of the spring and fall Inter-Tropical Convergence Zone (ITCZ) noted by many investigators (e.g., Lau and Chan 1983; Meehl 1987; Yatsunari 1991; Matsumoto and Murakami 2000, 2002; Hung et al. 2004).

The cause of this asymmetry has not been fully understood. A possible factor lies in the difference in the strength of broad-scale Walker circulation driven by zonal SST gradients over both the equatorial Pacific and Indian Oceans. Over the Pacific, the Walker circulation that gives rising motion over the Maritime Continent is affected by the intensity of the eastern equatorial Pacific cold tongue (Wang 1994, Li and Philander 1996). The cold tongue is most intense in boreal fall, so the Pacific Walker cell may favor convection over the Maritime Continent in boreal fall rather than boreal spring. Across the equatorial Indian Ocean the zonal SST gradient is more favorable for a local Walker type circulation that supports convection over the Maritime Continent in boreal fall than in boreal spring, as the annual cycle of the western equatorial Indian Ocean is warmest in boreal spring (Webster et al. 1998). As a result, the planetary scale circulation may favor enhanced convection over the land bridge of South East Asia/Maritime Continent in boreal fall and thus a continuous southeastward march from Asian summer monsoon to Australian summer monsoon, and may make the reverse trip harder during boreal spring.

More direct hypotheses to explain the asymmetry have been proposed by several investigators. Matsumoto and Murakami (2000) suggested the asymmetry is due to the fact that cold surges that originate from the high terrain of Asian continent during boreal fall are stronger than the cold surges that originate from Australia during boreal spring. Matsumoto and Murakami (2002) also proposed that this asymmetry is related to the different equatorial basic flows in the western Pacific and Indian Ocean, and their respective annual variations. They suggested that the western equatorial Pacific with a strong Kelvin-type mean flow during boreal fall allows the convection to move southward, and that the flow weakens during boreal spring such that it inhibits the return

journey during boreal fall. They also suggested that the variation of a complex Rossby-type mean flow in equatorial Indian Ocean allows convection to move northward in boreal spring but inhibits the southward movement in boreal fall.

Hung et al. (2004) proposed that the northward march of the ITCZ during boreal spring is blocked by subsidence in oceanic regions to the west of heat sources (India, Indochina, and the Philippines). They suggested that this subsidence, which is similar to that occurring west of Tibetan Plateau during the summer monsoon (Yanai et al. 1992), is the result of the Rossby-wave response in the monsoon-desert mechanism suggested by Rodwell and Hoskins (1996). Tim Li (2003, personal communication) proposed that the asymmetry is attributed to an internal atmospheric dynamics mechanism by which equatorial oceanic convection tends to propagate eastward due to the production of a boundary layer convergence to the east of the deep convection. Such a process will favor the southeastward seasonal march from the Asian summer monsoon to the Asian winter monsoon, but not the northwestward march from the Australian region to the Asian summer monsoon.

Our analysis suggests that at least a part of this asymmetry is due to a combination of two effects: (i) the low-level wind and terrain interactions throughout the region during boreal fall that do not have counterparts in boreal spring, and this includes the effect of boreal fall cold surges noted by Matsumoto and Murakami (2002); and (ii) an intervening region between the equator and 20°N in the longitudes of Southeast Asia and the Maritime Continent that in the low levels has a convergence bias in boreal fall and a divergence bias in boreal spring. Over the eastern Indian Ocean, this effect is enhanced by the beta effect of the equatorial zonal wind near the surface. Both effects can be

related to the SLP differences between spring and fall that appear to be the result of the global-scale mass redistribution between the land and ocean regions, which is driven by their different thermal memories. Because of the orientation of the Asian and Australian landmasses, this redistribution facilitates the southeastward march of maximum convection from the Asian summer monsoon to the Asian winter (Australian summer) monsoon, but it deters the reverse march in boreal spring.

Acknowledgements

We wish to thank Tim Li for stimulating discussions and Russ Elsberry and Pat Harr for reading the manuscript. This work was supported by the National Oceanic and Atmospheric Administration under Grant NA01AANRG0011 and the National Science Foundation under Grant ATM-0101135 at the Naval Postgraduate School.

References

- Aldrian, E, and D. Susanto, 2003: Identification of three dominant rainfall regions within Indonesia and their relationship to sea surface temperature. *Intl. J. Climatology*, **23**, 1435-1452.
- _____, L. Dumenil-Gates, and F. H. Widodo, 2003: Variability of Indonesian rainfall and the influence of ENSO and resolution in ECHAM4 simulations and in the reanalyses. Report No. 346, Max-Planck Institute for Meteorology, Hamburg, Germany.
(http://www.mpimet.mpg.de/de/web/download.php?src=max_scirep&file=pdfupload&id=350&filename=Rep346.pdf)
- Braak, C., 1921-29: Het Climaat van Nederlandsch Indie. *Magnet. Meteorol. Observ. Batavia, Verhand* No. **8**. (from Ramage, 1971).
- Chang, C.-P., P. A. Harr, and H. J. Chen, 2004a: Synoptic disturbances over the equatorial South China Sea during boreal winter. *Mon. Wea. Rev.*, in press.
- _____, _____, J. McBride, and H. H. Hsu, 2004b: Maritime Continent monsoon: Annual cycle and boreal winter variability. *East Asian Monsoon*, World Scientific Pub. Co., Singapore, in press.
- _____, C. H. Liu, and H. C. Kuo, 2003: Typhoon Vamei: An equatorial tropical cyclone formation. *Geophys. Res. Lett.*, **30**, 501-4.
- Coronas, Rev. J., 1912: The extraordinary drought in the Philippines, October 1911 to May 1912. Govt. Philippines Islands, Weather Bureau, Manila Bureau of Printing., 19pp.

- Cressman, G. P., 1959: An operational objective analysis system. *Mon. Wea. Rev.*, **87**, 367- 374.
- Flores, J.F. and V.F. Balagot, 1969: Climate of the Philippines. Chapter 3 of *Climates of Northern and Eastern Asia*. World Survey of Climatology, Vol.8., H. Arakawa (Editor), Elsevier Publishing Co., 159-213.
- Hamada, J.-I., M. D. Yamanaka, J. Matsumoto, S. Fukao, P. A. Winarso and T. Sribimawati, 2002: Spatial and temporal variations of the rainy season over Indonesia and their link to ENSO. *J. Meteor. Soc. Japan*, **80**, 285-310.
- Haylock, M. and J. McBride, 2001: Spatial and coherence and predictability of Indonesian wet season rainfall. *J. Climate*, **14**, 3882-3887.
- Hung, C.-W. and M. Yanai, 2004: Factors contributing to the onset of the Australian summer monsoon. *Quart. J. Roy. Meteor. Soc.*, **130**, 739-761.
- _____, X. Liu, and M. Yanai, 2004: Symmetry and asymmetry of the Asian and Australian summer monsoons. *J. Climate*, in press.
- Johnson, R.H., and R.A. Houze, Jr., 1987: Precipitating cloud systems of the Asian monsoon. *Monsoon Meteorology*, C.-P. Chang and T. N. Krishnamurti (Eds.), Oxford University Press, No. 7, 298-353.
- Kirono, D., N. Tapper, and J. McBride, 1999: Documenting Indoensian rainfall in the 1997/1998 El Nino event. *Phys. Geogr.*, **20**, 422-435.
- Lau, K. M. and P. H. Chan, 1983: Short-term climate variability and atmospheric teleconnections from satellite-observed outgoing longwave radiation. Part II: Lagged correlations. *J. Atmos. Sci.*, **40**, 2751-2767.

- Leise, J. A., 1982: A multidimensional scale-telescoped filter and data extension package. *NOAA Tech. Memo. ERL WPL-82*, 19 pp.
- Li, T., and S. G. H. Philander, 1996: On the annual cycle of the eastern equatorial Pacific. *J. Climate*, **9**, 2986-2998.
- Liu, W. T., 2002, Progress in scatterometer application, *J. Oceanogr.*, **58**, 121-136.
- Masó, Rev. M. S., 1914: Annual amount and distribution of rainfall in the Philippines. Govt. Philippines Islands, Weather Bureau, Manila Bureau of Printing., 42pp.
- Matsumoto, J., 1992: The seasonal changes in Asian and Australian monsoon regions. *J. Meteor. Soc. Japan*, **70**, 257-273.
- _____, and T. Murakami, 2000: Annual changes of tropical convective activities as revealed from equatorial symmetric OLR Data. *J. Meteor. Soc. Japan*, **78**, 543-561.
- _____, and _____, 2002: Seasonal migration of monsoons between the Northern and Southern Hemisphere as revealed from equatorially symmetric and asymmetric OLR data. *J. Meteor. Soc. Japan*, **80**, 419-437.
- McBride, J., 1987: The Australian summer monsoon. *Monsoon Meteorology*, C.-P. Chang and T. N. Krishnamurti (Eds.), Oxford University Press, 203-231.
- _____, 1998: Indonesia, Papua New Guinea, and Tropical Australia: The Southern Hemisphere monsoon. *Meteorology of the Southern Hemisphere, Meteorological Monographs*, **49**, American Meteorological Society, 89-99.
- _____, N.E. Davidson, K.Puri, and G.C Tyrrell, 1995: The flow during TOGA COARE as diagnosed by the BMRC-tropical analysis and prediction system. *Mon. Wea. Rev.*, **123**, 717-736.

- Meehl, G. A., 1987: The annual cycle and interannual variability in the tropical Pacific and Indian Ocean regions. *Mon. Wea. Rev.*, **115**, 27-50.
- Neumann, C. J., 1993: Global overview. *Global Guide to Tropical Cyclone Forecasting*. WMO/TD-No. 560, World Meteorological Organization, Geneva, Switzerland, 1.1-1.56.
- Qian, W. and D. K. Lee, 2000: Seasonal march of Asian Summer Monsoon. *Int. J. Climatol.*, **20**, 1371-1386
- Ramage, C. S., 1968: Role of a tropical “maritime continent” in the atmospheric circulation. *Mon. Wea. Rev.*, **96**, 365-369.
- Ramage, C. S., 1971: *Monsoon Meteorology*. Acad. Press, 296pp.
- Riehl, H., 1954: *Tropical Meteorology*. McGraw-Hill Book Co., 392pp.
- Rodwell, M. J., and B. J. Hoskins, 1996: Monsoons and the dynamics of deserts. *Quart. Roy. Meteor. Soc.*, **122**, 1385-1404.
- Schmidt, F. H. and J. H. A. Ferguson, 1951: Rainfall types based on wet and dry period ratios for Indonesia with western New Guinea. *Verhandelingen*, **42**, 77pp plus figures (from McBride, 1998).
- Simpson, J., C. Kummerow, W. - K. Tao and R.F. Adler, 1996: On the Tropical Rainfall Measuring Mission (TRMM). *Meteor. Atmos. Phys.*, **60**, 19-36.
- Sukanto, M., 1969: Climate of Indonesia. *World Survey of Climatology*, H. Arakawa, Ed., Vol. **8**, *Climates of Northern and Eastern Asia*. Elsevier, 215-229.
- van den Dool, H. M., S. Saha, 1993: Seasonal redistribution and conservation of atmospheric mass in a general circulation model. *J. Climate*, **6**, 22-30.

- van Loon, H, 1967: The half yearly oscillation in middle and high southern latitudes and the colorless winter. *J. Atmos. Sci.*, **24**, 472-486.
- Waliser, D.E and C. Gautier, 1993: A satellite-derived climatology of the ITCZ. *J. Climate*, **6**, 2162-2174.
- Wang, B., 1994: On the annual cycle in the tropical eastern and central Pacific. *J. Climate*, **7**, 1926-1942..
- Webster, P. J., T. Palmer, M. Yanai, R. Tomas, V. Magana, J. Shukla and T. Yasunari, 1998: Monsoons: Processes, Predictability and the prospects for prediction. *J. Geophys. Res.*, **103**,14451-14,510.
- Wyrтки, K., 1956: The rainfall over the Indonesian waters. *Kementerian Perhubungan Lembaga Meteorologi dan Geofisik Verhand*, No. **49**. (from Ramage, 1971).
- Yanai, M., C. Li, and Z. Song, 1992: Seasonal heating of the Tibetan Plateau and its effects on the evolution of the Asian summer monsoon. *J. Meteor. Soc. Japan*, **70**, 319-351.
- Yasunari, T., 1991: The monsoon year - a new concept of the climatic year in the tropics. *Bull. Amer. Meteor. Soc.*, **72**, 1331-1338.

Figure Captions

Fig. 1. Monthly mean rainfall and topography for (a) January, (b) April, (c) July, and (d) October (from Chang et al., 2004b).

Fig. 2. The annual cycle mode at rainfall stations. The phase of the cycle is shown as a 12-month clock with a northward arrow indicating maximum rainfall in January. The arrows rotate clockwise with eastward, southward and westward arrows indicating April, July and October, respectively. The length of the arrow defines the amplitude of the cycle. This figure also serves to show the locations of the observation stations for the monthly rainfall data sets used in this study.

Fig. 3. Mean QuikSCAT wind for January (black) and July (red), and topography (m).

Fig. 4. The annual cycle mode (black) and the month and amount of the maximum monthly rainfall (gray) for the objectively-analyzed gridded rainfall. Black dots indicate grid points where the amplitude of the annual cycle mode is no more than 40% of the maximum rainfall and the phase difference is at least two months.

Fig. 5. The semiannual cycle mode (dark bar), overlapped with the annual cycle mode, for the objectively-analyzed gridded rainfall. Data are plotted if the amplitude of the semiannual cycle is at least 80% of that of the annual cycle. Each bar is centered at the grid point and pointing in the two (opposite) directions of the semiannual cycle peaks. The entire length of the bar is twice the length of an annual cycle vector with the same amplitude. See text for details. Example of rainfall time series (mm day^{-1}) at grid points where the semiannual cycle is important (5°N , 100°E), the annual cycle is important (8°S , 110°E), and neither is important (3°S , 133.5°E) are shown in the upper-right insert.

Fig. 6. Comparisons of annual cycles deduced from TRMM PR vs. analyzed rainfall. The direction of vector shows the phase difference in a 12-month clock. A northward pointing arrow means the two annual cycles are exactly in phase, and a westward (eastward) pointing arrow means the TRMM PR annual cycle mode leads (lags) the analyzed rainfall mode by three months. Gray arrows mean the amplitude of TRMM PR mode is larger and black arrows mean it is smaller.

Fig. 7. Differences of TRMM PR rainfall and QuikSCAT winds between boreal winter and boreal summer (DJF minus JJA). Warm colors are the boreal summer monsoon regime and cool colors are the boreal winter monsoon regime. See text for details.

Fig. 8. Monsoon regimes during transition seasons deduced from TRMM PR rainfall. A grid point is identified if the rainfall during one of the two transition seasons is the maximum in the annual cycle, and the value plotted is the difference between this transition-season rainfall and the boreal winter and or boreal summer whichever is highest. Warm colors are the boreal fall monsoon regime and cool colors are the boreal spring monsoon regime. There are large areas of zero value indicating that maximum rainfall occurs outside of spring and fall. These areas are plotted with the lightest warm color. The difference of QuikSCAT winds between the two transition seasons (SON minus MAM) is plotted for the entire domain. See text for details.

Fig. 9. Differences of sea-level pressure between boreal fall and boreal spring (SON minus MAM, warm colors positive, cool colors negative). Unit: hPa. Higher values over land areas at high latitudes are truncated because they may be affected artificially by the surface to sea level conversion. The rectangular box is an insert

region covering the domain of Fig. 10. Areas where values do not meet the 5% significance test are indicated by black dots.

Fig. 10. Differences of sea-level pressure between boreal fall and boreal spring (SON minus MAM), for the insert region to Fig. 9. Negative isobars are dotted and the zero line is dashed. Unit: hPa. Schematics of sea-level wind differences based on the differences in the sea-level pressure pattern are indicated. The elliptic-shaped area indicates preferred belt of convergence in fall and divergence in spring. See text for details.

Monthly Mean Rainfall

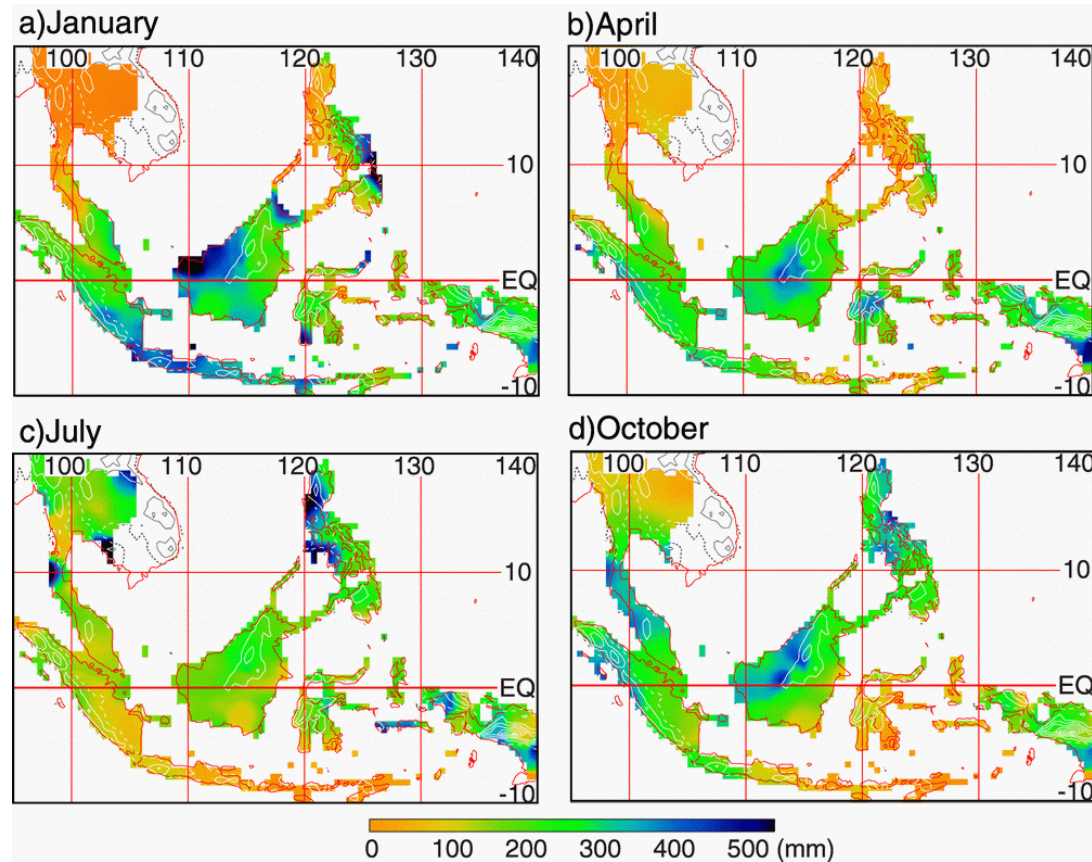


Fig. 1

Fig. 1. Monthly mean rainfall and topography for (a) January, (b) April, (c) July, and (d) October (from Chang et al., 2004).

Annual Cycle Mode at Rainfall Stations

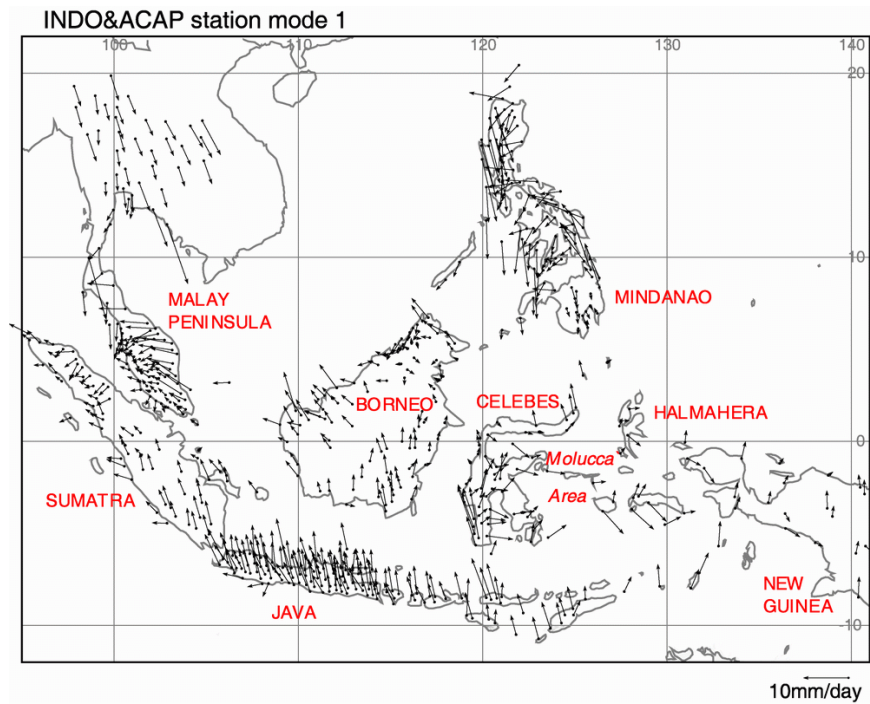


Fig. 2. The annual cycle mode at rainfall stations. The phase of the cycle is shown as a 12-month clock with a northward arrow indicating maximum rainfall in January. The arrows rotate clockwise with eastward, southward and westward arrows indicating April, July and October, respectively. The length of the arrow defines the amplitude of the cycle. This figure also serves to show the locations of the observation stations for the monthly rainfall data sets used in this study.

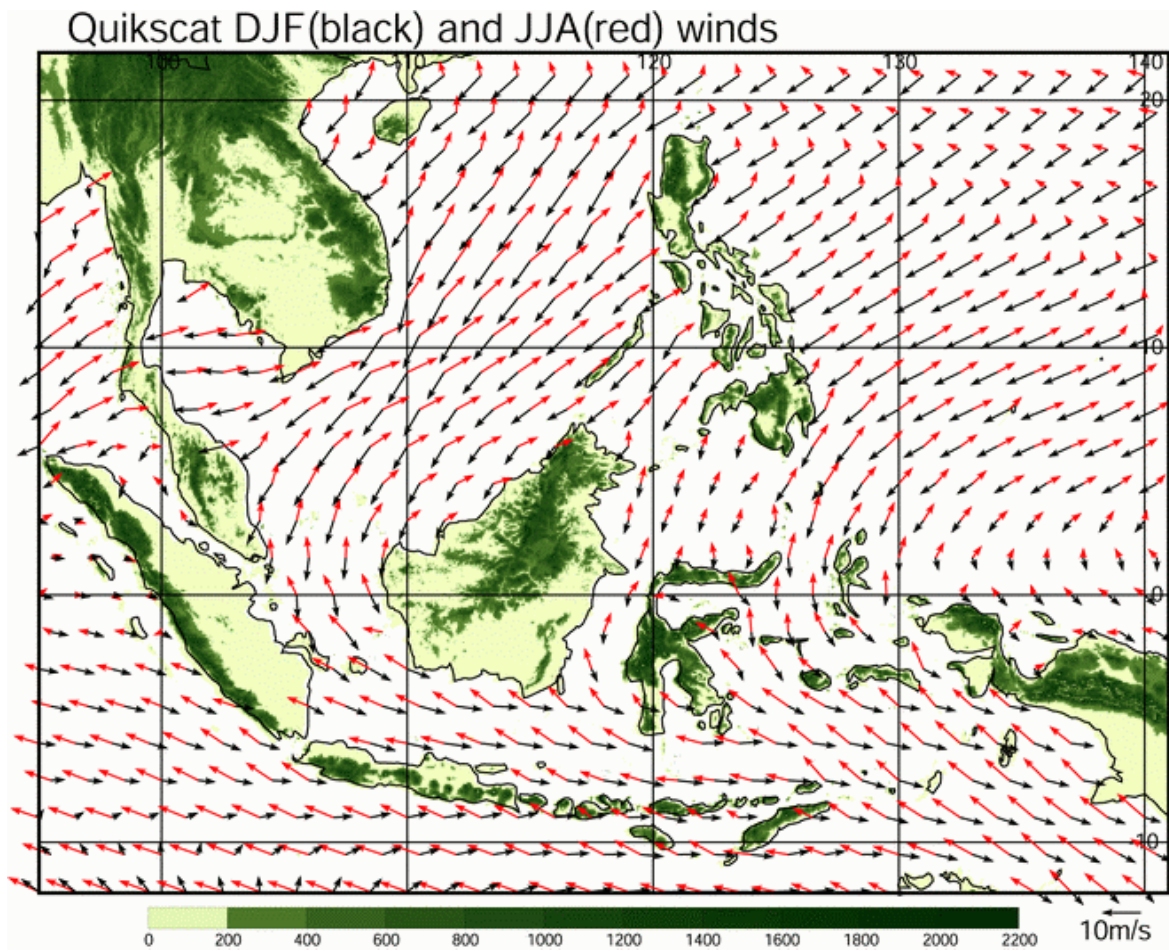


Fig. 3. Mean QuikSCAT wind for January (black) and July (red), and topography (m)..

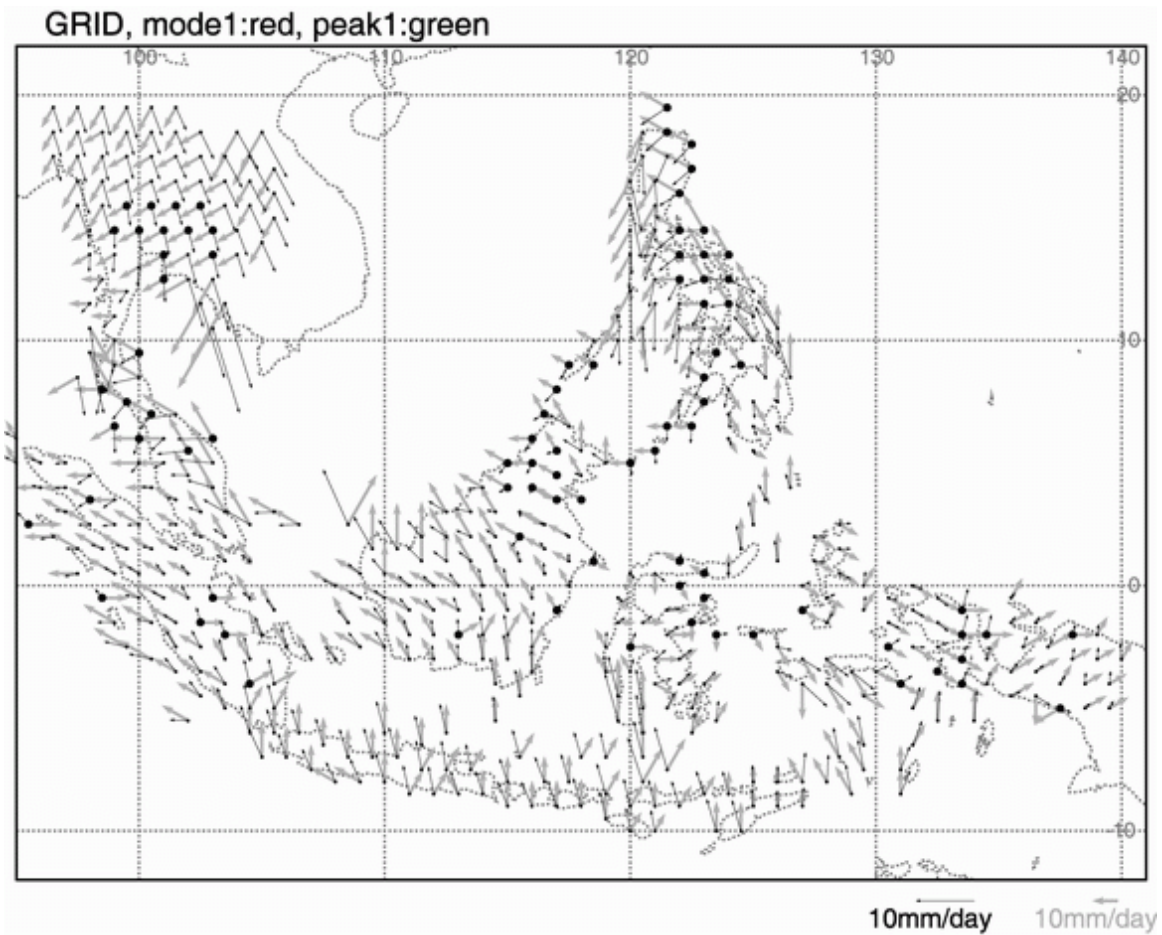


Fig. 4. The annual cycle mode (black) and the month and amount of the maximum monthly rainfall (gray) for the objectively-analyzed gridded rainfall. Black dots indicate grid points where the amplitude of the annual cycle mode is no more than 40% of the maximum rainfall and the phase difference is at least two months.

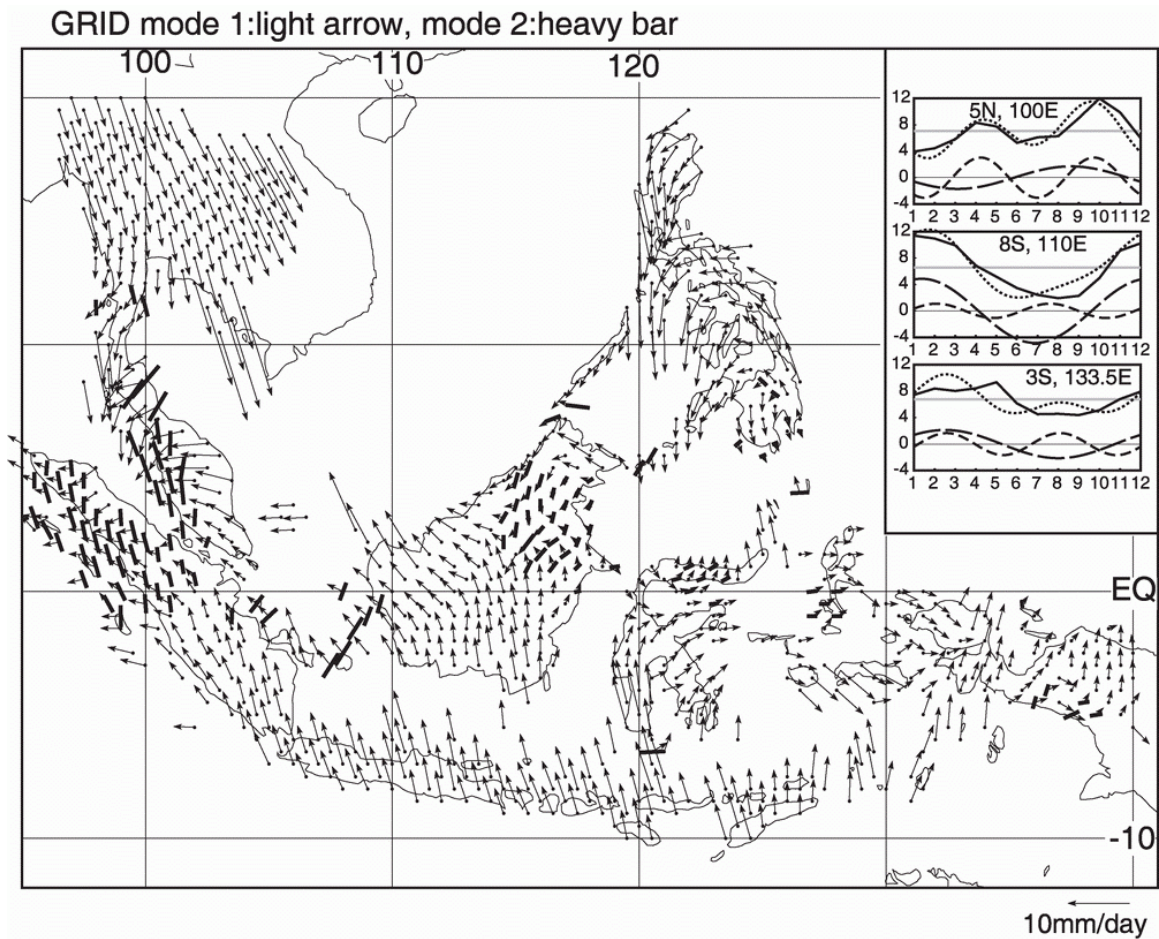


Fig. 5. The semiannual cycle mode (dark bar), overlapped with the annual cycle mode, for the objectively-analyzed gridded rainfall. Data are plotted if the amplitude of the semiannual cycle is at least 80% of that of the annual cycle. Each bar is centered at the grid point and pointing in the two (opposite) directions of the semiannual cycle peaks. The entire length of the bar is twice the length of an annual cycle vector with the same amplitude. See text for details. Example of rainfall time series (mm day⁻¹) at grid points where the semiannual cycle is important (5°N, 100°E), the annual cycle is important (8°S, 110°E), and neither is important (3°S, 133.5°E) are shown in the upper-right insert.

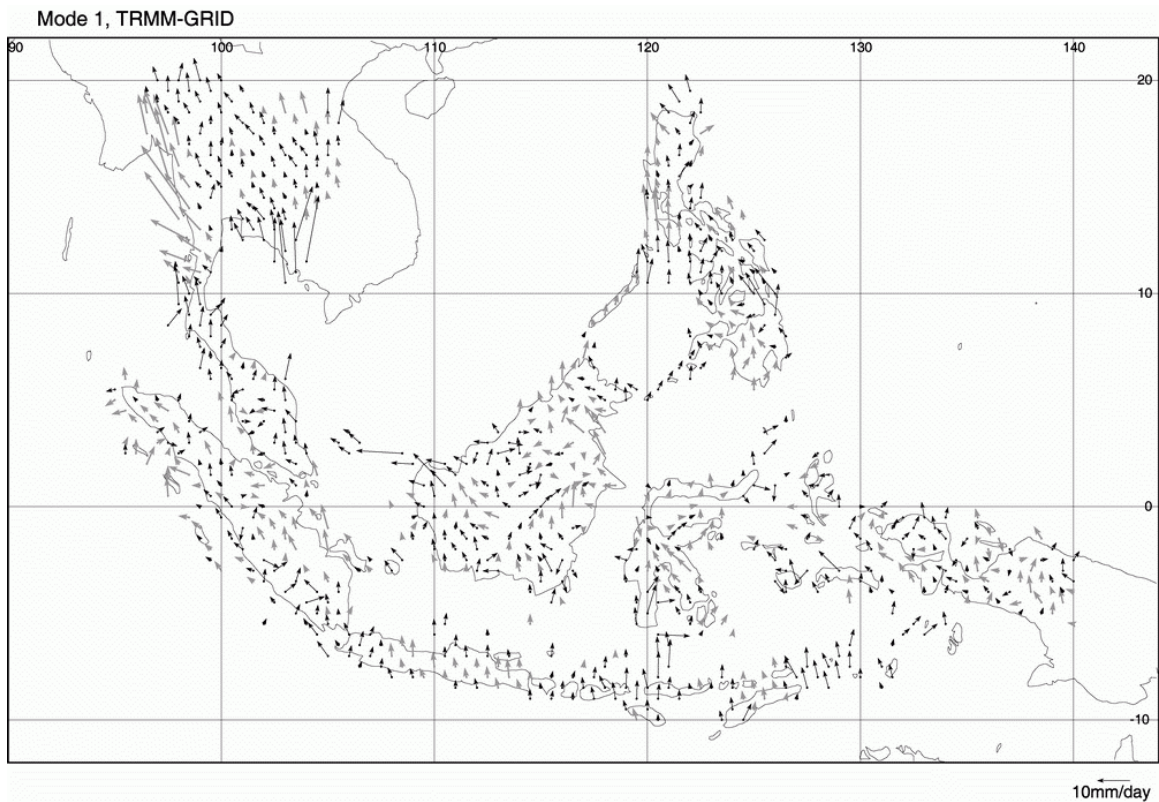


Fig. 6. Comparisons of annual cycles deduced from TRMM PR vs. analyzed rainfall.

The direction of vector shows the phase difference in a 12-month clock. A northward pointing arrow means the two annual cycles are exactly in phase, and a westward (eastward) pointing arrow means the TRMM PR annual cycle mode leads (lags) the analyzed rainfall mode by three months. Gray arrows mean the amplitude of TRMM PR mode is larger and black arrows mean it is smaller.

DJF-minus-JJA TRMM PR(mm/day) and Quikscat winds

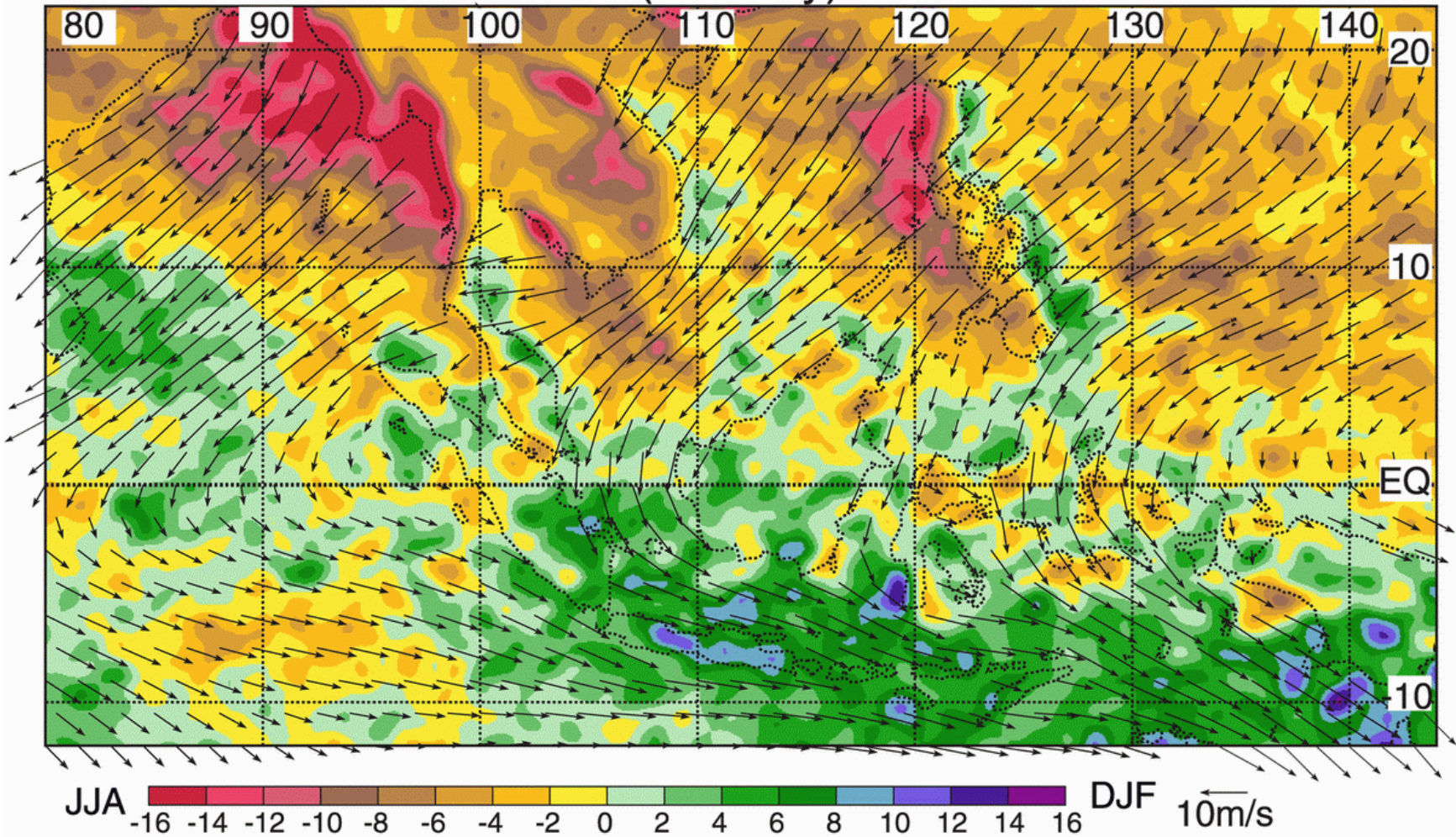


Fig. 7. Differences of TRMM PR rainfall and QuikSCAT winds between boreal winter and boreal summer (DJF minus JJA). Warm colors are the boreal summer monsoon regime and cool colors are the boreal winter monsoon regime. See text for details.

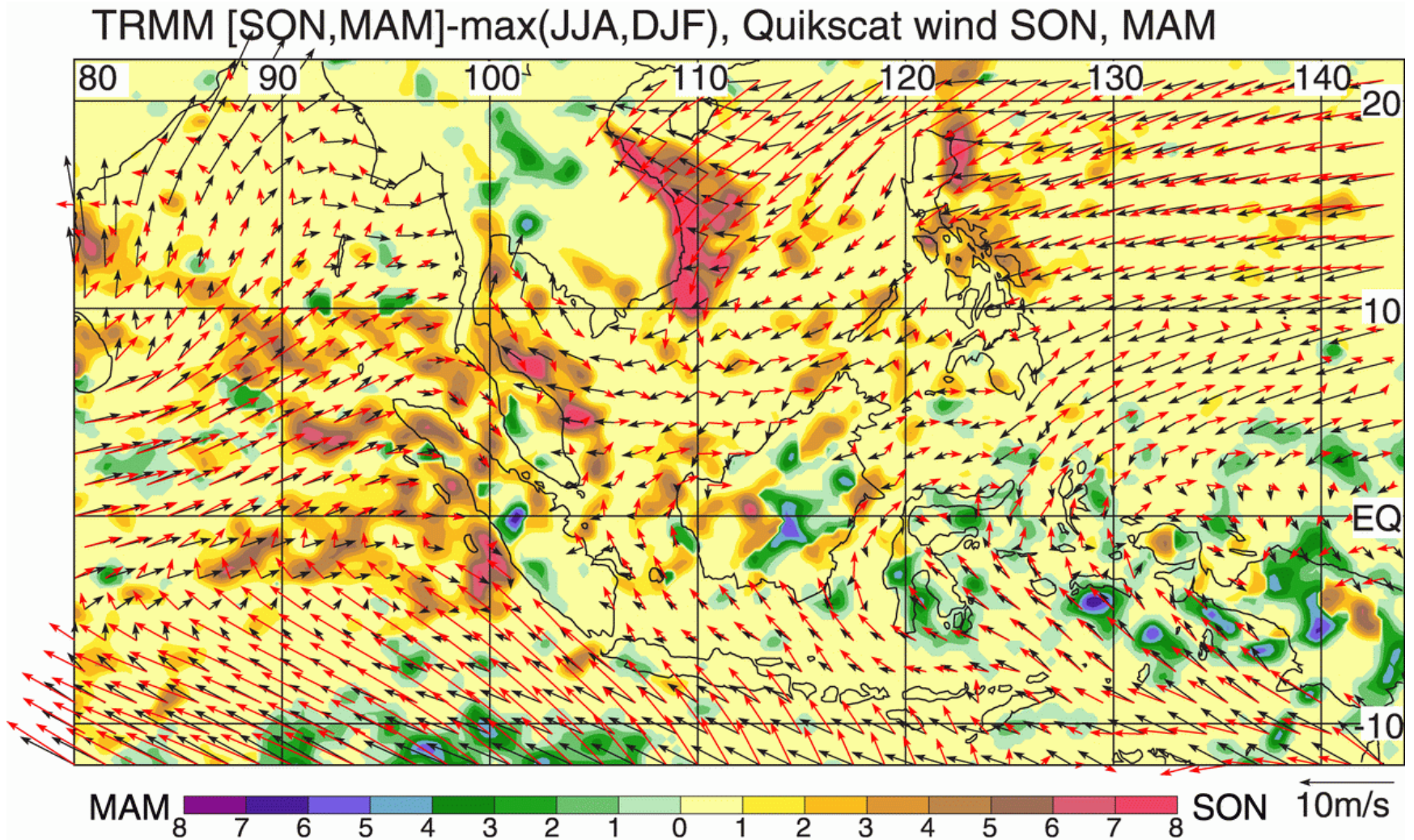


Fig. 8. Monsoon regimes during transition seasons deduced from TRMM PR rainfall. A grid point is identified if the rainfall during one of the two transition seasons is the maximum in the annual cycle, and the value plotted is the difference between this transition-season rainfall and the boreal winter and or boreal summer whichever is highest. Warm colors are the boreal fall monsoon regime and cool colors are the boreal spring monsoon regime. The difference of QuickSCAT winds between the two transition seasons (SON minus MAM) is plotted for the entire domain. See text for details.

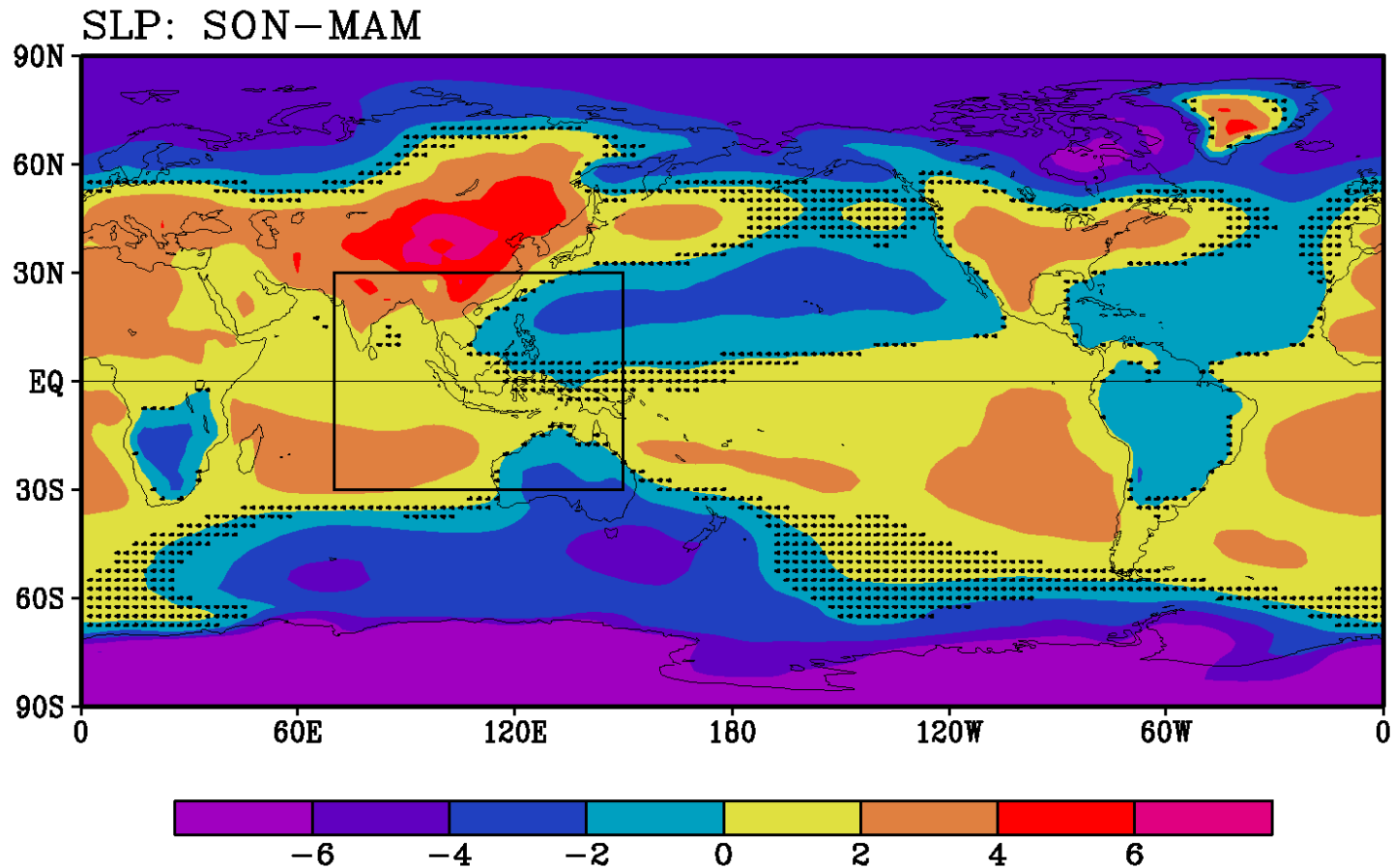


Fig. 9. Differences of sea-level pressure between boreal fall and boreal spring (SON minus MAM, warm colors positive, cool colors negative). Unit: hPa. Higher values over land areas at high latitudes are truncated because they may be affected artificially by the surface to sea level conversion. The rectangular box is an insert region covering the domain of Fig. 10. Areas where values do not meet the 5% significance test are indicated by black dots.

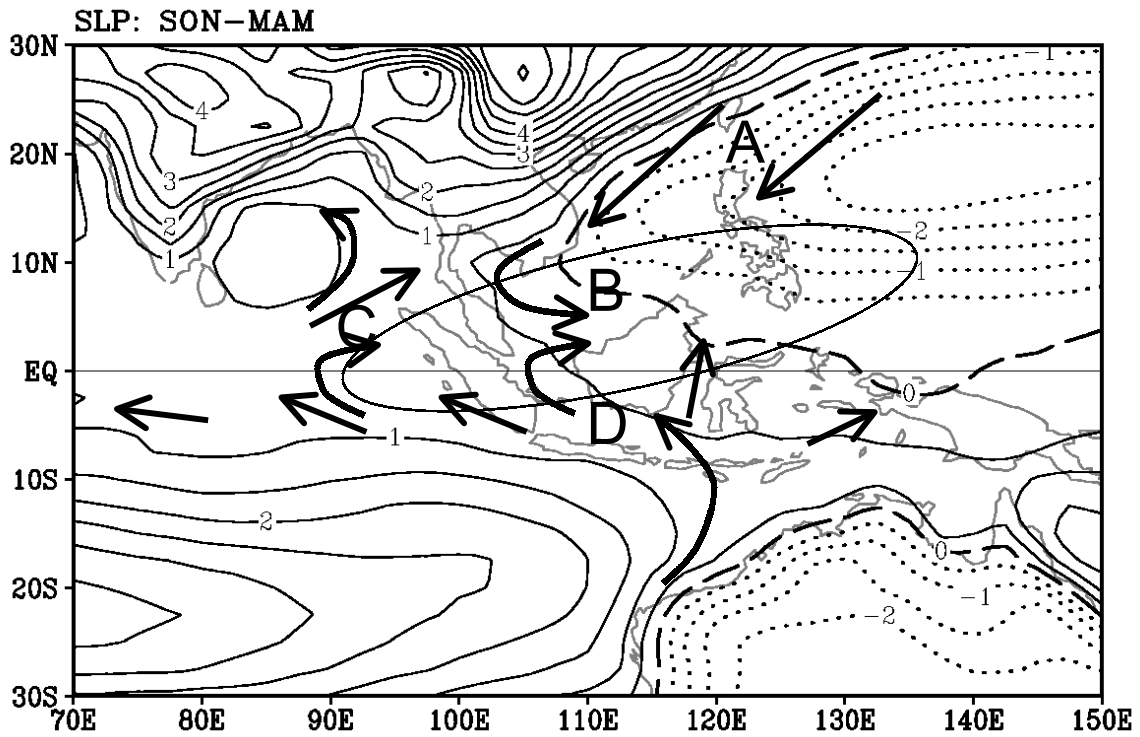


Fig. 10. Differences of sea-level pressure between boreal fall and boreal spring (SON minus MAM), for the insert region to Fig. 9. Negative isobars are dotted and the zero line is dashed. Unit: hPa. Schematics of sea-level wind differences based on the differences in the sea-level pressure pattern are indicated. The elliptic-shaped area indicates preferred belt of convergence in fall and divergence in spring. See text for details.